High-Temperature Interactions of Metal Oxides and a PVDF Binder

Miles C. Rehwoldt,[§] Yujie Wang,[§] Feiyu Xu, Pankaj Ghildiyal, and Michael R. Zachariah*

Read Online

ACCESS | Metrics & More | Article Recommendations | Supporting Information

ABSTRACT: Interactions between energetic material relevant nanoscale metal oxides (SiO_2, TiO_2, MgO, Al_2O_3, CuO, Bi_2O_3) and poly(vinylidene fluoride) (PVDF) at high temperature were investigated by temperature-jump/time-of-flight mass spectrometry (T-jump/TOFMS) and thermogravimetric-differential scanning calorimetry (TGA-DSC). Scanning electron microscopy (SEM) and transmission electron microscopy (TEM) were used to characterize the morphology of the compositions, while X-ray diffraction (XRD) was utilized to analyze the condensed phase crystalline species at temperatures of interest. The exergonicity and exothermicity of HF gas with hydroxyl-terminated metal oxide surfaces make HF the likely fluorine-bearing moiety and primary mode of the fluorinating reactions, where terminal OH⁻ configurations are replaced by F⁻ in the formation of a stronger metal–fluorine bond. However, not all compositions produce corresponding stable metal fluoride. The results show that while some of the investigated metal oxide–PVDF compositions enhance PVDF decomposition and release HF in larger quantities than PVDF, others release HF in smaller quantities than PVDF and even retard PVDF decomposition. The former compositions demonstrate exothermic, multistep mass loss modes prior to neat PVDF mass loss, and the relative intensity of HF gas increases as the temperature of the release point decreases, implying a correlation between HF release and the progression of exothermic behavior. An interplay dynamic where surface interactions both lower the onset of HF release and engage exothermically with HF gas subsequently is proposed.

KEYWORDS: PVDF, polymer composites, mass spectrometry, rapid heating, nanoparticles

$$HF\ ratio = \frac{HF_{max}}{HF_{max\ (PVDF)}}$$
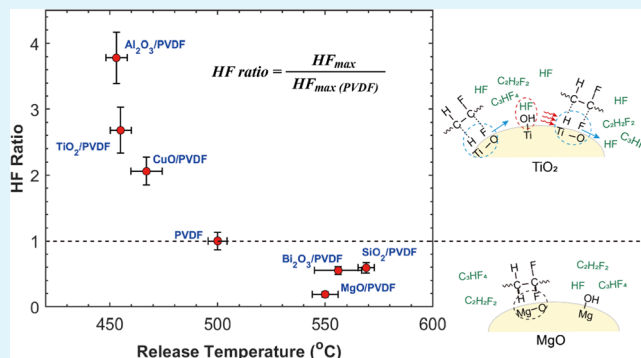
1. INTRODUCTION

Binders in energetic formulations play a central role in the ability to fabricate practical compositions for a variety of propellent applications. Polymer binders are commonly employed to hold the fuel and oxidizer in close proximity so as not to impede reactivity and maintain mechanical integrity to withstand mechanical stresses. The fluoropolymer poly-(vinylidene fluoride) (PVDF; 59 wt % F) is an interesting material in its capability to serve as both a binder and potential oxidizer. Furthermore, PVDF has a low melting point (≈150 °C) and is highly soluble in compatible polar organic solvents, such as dimethylformamide (DMF), which makes it attractive for use in contemporary additive manufacturing methods in rapid prototyping of material architectures.[1–4]

Heterogeneous reactive materials are compositions that are typically comprised of a metallic fuel and a metal oxide oxidizer. In this study, we focus on the composites of nanoscale metal oxides and PVDF to report on their chemical interactions. While past studies have highlighted the ability of some metal oxides to affect the mechanical wear,[5] crystal structure, and electroactive behavior of PVDF (α-phase vs β-phase),[6–8] we assess this relationship with respect to how PVDF may act as an acidic oxidizer in the presence of a variety of potential metal fuels[9–12] for the exothermic production of

volatile metal fluorides (e.g., SiF_4, AlF_3, TiF_4, MgF_2, etc.).[13] PVDF-based energetic systems typically contain nanoscale aluminum as a metal fuel, where prior studies have shown there to be a potentially unique preignition reaction (PIR) at the interface of the fluoropolymer and hydroxyl-terminated native aluminum oxide shell (3−4 nm thick). The native shell facilitates early-onset release of the PVDF pyrolysis product—HF gas—at elevated temperatures (>300 °C)[14] as it etches the alumina shell and further exposes the aluminum core to fluorination.[2,15–18] The temperature and rate at which HF gas is released and exothermicity of its reaction with the oxide shell have all been proposed to be rate-limiting steps in the overall reaction rate of PVDF fluorinated metal nanoparticles.[15,17–19]

Due to the prevalence of aluminum in energetic formulations, the aluminum oxide interaction with PVDF has been the primary system of study. The goal of this work is to broaden the scope of study and investigate general trends in
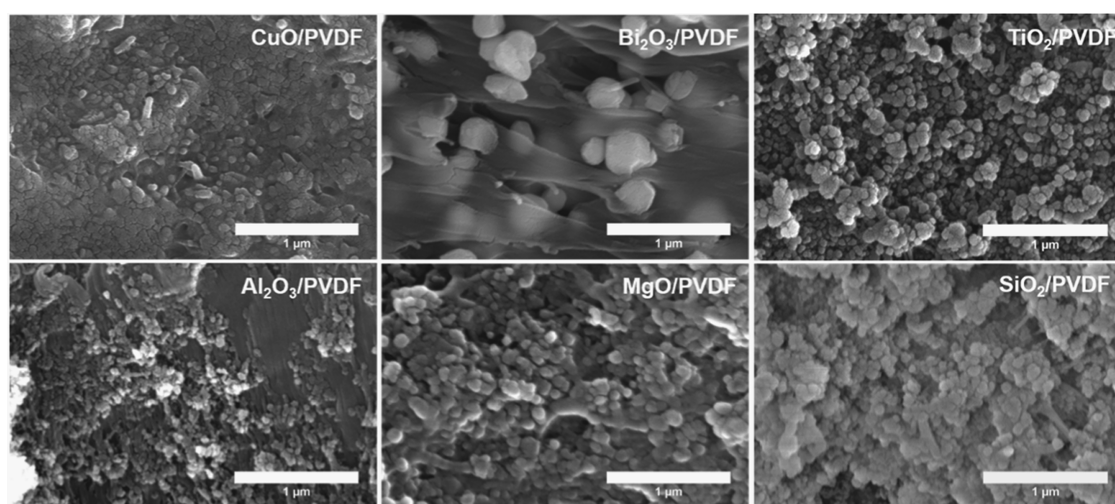
Figure 1. SEM cross sections of all metal oxide/PVDF thin-film compositions illustrating metal oxides encapsulated within the PVDF matrix.

high temperature, rapid heating pyrolysis of PVDF with other nanoscale metal oxides which make up the native oxide shell of less studied metal fuels (e.g., SiO_2, TiO_2, MgO, etc.). Relevant metal oxides commonly utilized as relatively strong oxidizers in nanoscale thermite (metal/metal oxide) formulations (e.g., CuO, Bi_2O_3) are also studied. The interaction with PVDF and metal oxide oxidizers has not been generally considered in past studies and is investigated further in this study.[3,20−22]

The transient technique of temperature-jump/time-of-flight (T-jump/TOFMS) is used as the primary diagnostic technique for monitoring the evolution of gas-phase species during and after a rapid heating event. T-jump/TOFMS synchronizes rapid heating ($\approx 10^5$ K/s) and gas-phase chemical speciation (10 kHz) to enable the characterization of metal oxide/PVDF chemistry under the rapid heating conditions expected in the combustion of analogous energetic systems.[23−25] T-jump/TOFMS is supplemented by traditional slow heating (10 °C/min) thermal analysis methods of thermogravimetric-differential scanning calorimetry (TGA-DSC) conducted in an anaerobic environment to account for the lack of thermal analysis capabilities of the T-jump/TOFMS beyond simple temperature measurements. Scanning electron microscopy (SEM) and transmission electron microscopy (TEM) are utilized to characterize both material length scales and morphology of the composition. Additionally, X-ray diffraction (XRD) is used as a method for the chemical characterization of condensed phase crystalline species at temperatures of interest with respect to TGA-DSC measurements.

2. EXPERIMENTAL METHODS

2.1. Materials. Nanoscale metal oxides of CuO (<50 nm), Al_2O_3 (<50 nm), and TiO_2 (≈ 21 nm) were purchased from Sigma-Aldrich (Millipore Sigma), while Bi_2O_3 (≈ 80 nm), MgO (≈ 50 nm), and SiO_2 (60−70 nm) were purchased from U.S. Research Nanomaterials, Inc. Poly(vinylidene fluoride) (PVDF, 59 wt % F, MW = 534 000 g/mol) powder was purchased from Sigma-Aldrich (Millipore Sigma), and N,N-dimethylformamide (DMF 99.8%) solvent was purchased from BDH Chemicals. All chemicals were used as received.

2.2. Thin-Film Sample Preparation. Samples studied were the thin-film compositions of nanoscale metal oxide particles within a PVDF binder. Combining and mixing of each of the binary systems was done through a wet process by which a thoroughly mixed polymer/particulate precursor solution is either drop cast onto a thin platinum wire for T-jump/TOFMS or dispensed onto a heated

substrate to allow for solvent evaporation and material solidification for free-standing structures.[21]

Each precursor solution was formulated by first dissolving 100 mg/mL PVDF in DMF and stirred for a minimum of 4 h. Each respective submicron powder was added to the polymer solution without any stoichiometric considerations but with sufficient loading to both enhance any potential intracomposition interactions and allow for ease of precursor dispensing in film preparation. Preliminary measurements showed no change in the onset of chemical interactions based on weight percentage; thus, only a single mass loading was considered in each case.[26] A mass loading of 50 wt % of submicron powder with respect to the polymer content was added to the polymer solution. The suspension was vortex mixed for 10 s using a Vortex Genie, ultrasonicated for 30 min to an hour, and physically stirred via a magnetic stir bar for 18−24 h.

The precursor suspension was treated as ink for direct-write, microextrusion additive manufacturing for the fabrication of batches of free-standing films of the composition, where the submicron powder is homogeneously embedded within the polymer binder.[21] A System 30M pressure-driven 3D printer (Hyrel 3D) extrudes the precursor ink from a 10 mL disposable syringe with a blunt 18 gauge Luer Lock dispensing needle in a layer-by-layer fashion onto a glass printing bed heated to 70 °C. The drying process is controlled by the temperature of the printing bed, the speed and extrusion rate of the print (0.5−5 mL/h), and the effectiveness of the solvent exhaust venting. Each subsequent layer is deposited after the previous layer has sufficiently dried. The resulting film thicknesses range between 7 and 10 μm per layer with most films having a thickness between 40 and 50 μm. Batches of rectangular sheets are printed from which multiple samples are harvested for use in different material analysis techniques (i.e., XRD, TGA-DSC, and SEM).

2.3. Nanoparticle and Composite Characterization. Particle sizes and film composition were characterized by transmission electron microscopy (Tecnai12) operating at 120 kV, scanning electron microscopy (NNS450) operating at 20 kV accelerating voltage, and X-ray diffraction crystallography (PANalytical Empyrean Series 2). Utilizing images from TEM and SEM, specifics of the particle sizes are analyzed. Quoted sizes are taken directly from the manufacturers and represent the average particle size or range of sizes. Figure S1 depicts aggregates of each metal oxide nanoparticle type through TEM, which show the differences in size, aggregation behavior (e.g., tightly packed CuO), and particle morphology. The observed sizes of the metal oxide particles are all less than 200 nm with many primary particles noticeably smaller (e.g., SiO_2) or larger (e.g., Bi_2O_3) than what they are quoted as being. It should also be noted that while most metal oxide particle types are spherical, some particle types contain different levels of rodlike architectures (i.e., Al_2O_3 and MgO). It is possible that the metal oxide particle size has
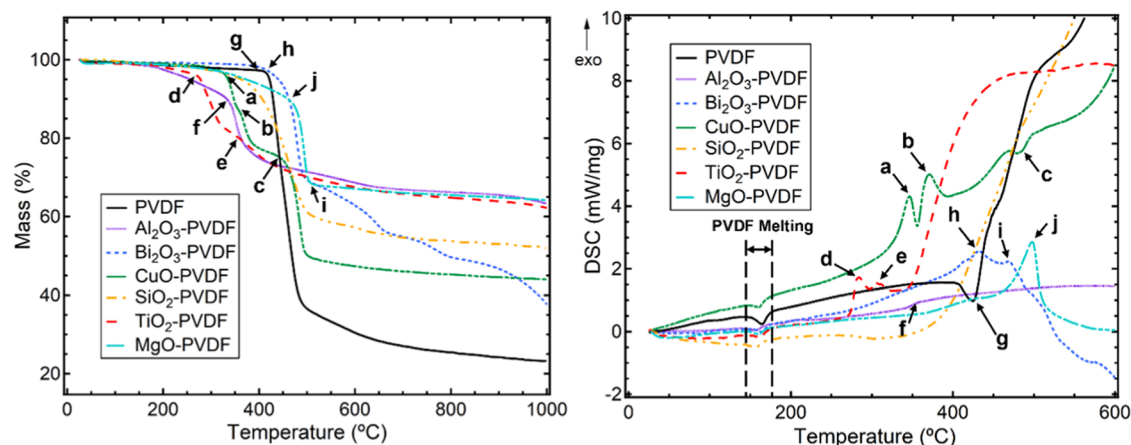
Figure 2. TGA-DSC of select metal oxide/PVDF thin films under an argon environment, heated at 10 °C/min.

an impact on the thermal decomposition of PVDF through changes in the interfacial contact area; however, this is outside the scope of this paper.

Noticeable differences in precursor suspension viscosity were observed due to differences in particle size and density of metal oxide nanoparticles when mixing with the PVDF-dissolved DMF solution. The variance in extrusion viscosity resulted in an expected reduction in structural, mechanical integrity as viscosity increased[21] but ultimately inconsequential with respect to the methods of analysis conducted in this study. SEM cross sections of the additively manufactured, homogeneously mixed metal oxide/PVDF thin films are shown in Figure 1. The images show the submicron architecture of film cross sections where larger individual particles or particle aggregates are distinguishable from the polymer matrix and with sizes that appear to be roughly one-to-one with the measured TEM length scales, suggesting that TEM particle sampling is likely representative of each respective particle size distribution.

2.4. Heating Experiments. *2.4.1. Thermogravimetric Analysis-Differential Scanning Calorimetry (TGA-DSC).* Temperature-resolved thermochemical analysis was conducted using a Netzsch STA 449 F3 Jupiter TGA-DSC operating in an argon environment with a flow rate of 70 mL/min. After conducting a correction run with an empty alumina pan, samples of each composition were loaded into the same open alumina pan and slowly heated from room temperature to 1000 °C at 10 °C/min. Initial acquisition of TGA-DSC profiles was utilized to pinpoint temperatures of interest for the iterative analysis of each material. TGA-DSC for each material was conducted in triplicate to ensure repeatability. Materials were arrested at the temperatures of interest and collected for XRD analysis.

2.4.2. T-Jump/Linear Time-of-Flight Mass Spectrometry. Rapid heating of metal oxide/polymer composites at ultrahigh heating rates was conducted via temperature-jump time of flight mass spectrometry (T-Jump/TOFMS), a technique described in greater detail by previous works.[25] The apparatus features a coupling of a linear time of flight mass spectrometer with a T-jump probe equipped with electrical feedthroughs and directly loaded into the vacuum environment of an ionization chamber (70 eV electron-gun) held at ~10^{-6} Torr. The technique of T-jump utilizes rapid resistive heating to simulate combustion time scale heating rates (>10^5 K/s), where the probe is prepared by soldering 6–12 mm of 76 μm diameter platinum wire (OMEGA Engineering Inc.) between the copper leads of the electrical feedthroughs. A single input trigger synchronizes resistive flash heating by a 3 ms pulse (4–14 V), gas-phase ionization for time-resolved speciation, and data collection (mass spectra intensity, time, voltage, current) by a LeCroy 600 MHz oscilloscope at a rate of 10 kHz over a 10 ms collection period. Additionally, the gas release of reaction products and intermediate species within the TOFMS chamber during chemical interactions of solid compositions is more apparent than would be detected in atmospheric conditions as the vacuum environment is devoid of molecular collisions necessary for

full chemical conversion. Electrical current readings are measured by a Teledyne LeCroy CP030A 30A 50 MHz current probe and combined with the oscilloscope measured voltage to experimentally determine resistance. Thermometry of the wire is obtained through the calibrated relationship between the temperature of the Pt wire and its resistance from the Callendar-Van Dusen equation. Several studies using this method have demonstrated the Pt wire reaching temperatures as high as ~1400 K at heating rates as rapid as ~10^6 K/s.[23,25] The temperature of wires with coated material is most accurate with a sufficiently small amount of thermal mass (<10 μm thick, 5–20 μg).[25]

In this experiment, samples are prepared by systematically drop casting a small coating of precursor solution onto platinum wires, which are then placed in a vacuum oven at 130 °C for 5 h to remove the remaining DMF solvent. Platinum wires with coated material of this type cannot be preflashed and thus require a surrogate wire with roughly the same dimensions to be flashed to get to the same approximate parameters before the experimental run. Measurements were repeated at least five times with raw data ported to MATLAB and processed through custom scripts to obtain calibrated mass spectra as a function of time and wire temperature.[25]

3. RESULTS AND DISCUSSION

3.1. Slow Heating Thermochemical Analysis. Thermochemical analysis of metal oxide/PVDF thin films was carried out by slow heating (10 °C/min) a thermogravimetric-differential scanning calorimeter in an anaerobic argon environment to supplement for the lack of gravimetric/calorimetric diagnostics of T-jump/TOFMS. An analysis was conducted in a comparative manner to the thermal behavior of a neat PVDF thin film. The results are displayed in Figure 2.

PVDF, represented by the solid black curve, shows the previously documented melting endotherm at 150 °C followed by a sharp endothermic/exothermic decomposition process at 422 °C (Figure 2g), which transitions to a more gradual decomposition mode. Volatile pyrolysis products largely consist of HF gas and fluorocarbon chain fragments from polymer chain cleavage accompanied by hydrogen transfer.[14,27,28] Prior TGA studies conducted in air have observed 100% mass loss after PVDF decomposition. In our case, however, the remaining residue does not interact with ambient argon, resulting in no further significant mass loss beyond ≈700 °C at roughly 20% mass remaining.[2]

Neat PVDF establishes the initial base thermochemical behavior of all compositions studied, where DSC measurements show PVDF melting occurring for all compositions within the range of 145–155 °C. The thermochemical
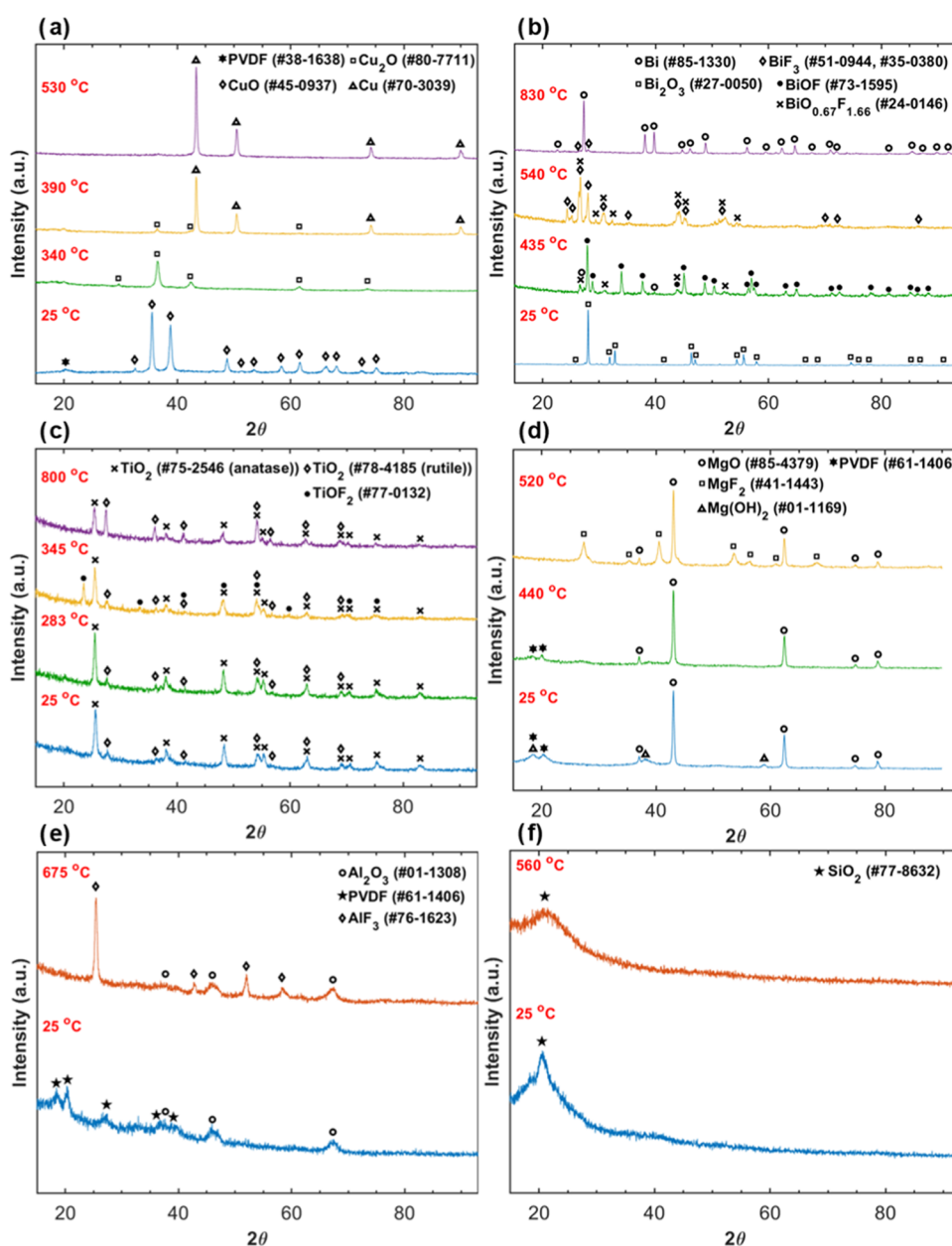
Figure 3. Temperature-dependent XRD analysis of condensed phase TGA-DSC-heated products of metal oxide/PVDF thin films: (a) CuO/PVDF, (b) Bi_2O_3/PVDF, (c) TiO_2/PVDF, (d) MgO/PVDF, (e) Al_2O_3/PVDF, and (f) SiO_2/PVDF.

behavior of each of the composites beyond 200 °C displays a unique TGA-DSC profile as major mass loss events are multistepped and straddle the primary decomposition of neat PVDF. Much of the more gradual mass loss behavior directly following 200 °C is attributed to dehydration of the high energy, high specific surface area of the metal oxide nanoparticles, and/or residual solvent evaporation. Material compositions of Al_2O_3/PVDF (Figure 2f), CuO/PVDF (Figure 2a,b), and TiO_2/PVDF (Figure 2d,e) demonstrate exothermic, multistep mass loss modes occurring as much as ≈150 °C prior to neat PVDF mass loss, while remaining exothermic and multistepped MgO/PVDF (Figure 2j) and Bi_2O_3/PVDF (Figure 2h,i) retard the primary mass loss mode attributed to the interaction of the metal oxide and PVDF during PVDF decomposition. SiO_2/PVDF appears to have little effect on the decomposition behavior of PVDF other than an earlier mass loss onset.

XRD was used to characterize the condensed phase products surrounding featured temperature points of exothermic and endothermic behavior identified by TGA-DSC. The results of this analysis are consolidated in Figure 3.

This analysis method has been previously conducted by Li et al. for CuO/PVDF, where we have reproduced the observations that the exotherms of Figure 2a,b at 332 and 364 °C correspond to transitions of CuO to Cu_2O and Cu_2O to Cu, respectively, as the released oxygen reacts with PVDF (Figure 3a). Each of these transitions coincides with the release of CO_2 with PVDF treated more as a fuel than an oxidizer in which CuO ultimately fully reduces to Cu simultaneous to the decomposition of the remaining PVDF at 469 °C (Figure 2c).[28] Aside from SiO_2/PVDF whose stable fluorine species, SiF_4 (SiF_3^+ when ionized), is gaseous at room temperature, the CuO/PVDF composition is the only composite that does not form any fluorine-containing compounds. Further XRD
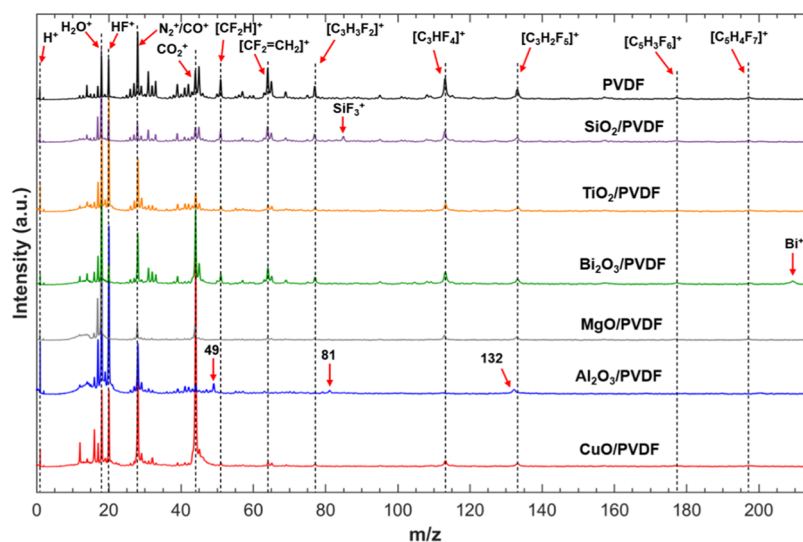
Figure 4. Averaged mass spectrum over a 10 ms collection period of rapidly heated Pt wires that are thinly coated with the selected metal oxide/PVDF compositions. The most notable mass species are labeled.

analysis of the temperature-dependent condensed phase progression shows that the five compositions of note (excluding SiO_2/PVDF) can be separated into three groups: (1) relatively simple, a fraction of the metal oxide fully transitions to the most stable, condensed phase fluorine compound (Al_2O_3/PVDF, MgO/PVDF), (2) complex, metastable fluorination/oxyfluoride progression (TiO_2/PVDF, Bi_2O_3/PVDF), and (3) no fluorination with enhanced reduction of the metal oxide compared to the neat metal oxide (CuO/PVDF). These three observed groups do not correlate with the temperature for which TGA-DSC observed interactions with PVDF will take place as the relatively early-onset interaction mass loss compositions (Al_2O_3/PVDF, TiO_2/PVDF, CuO/PVDF) are spread out throughout each of these proposed groups.

To better understand the observed fluorination behavior and onset point of the interaction of PVDF, mechanisms of aluminum fluorination by PVDF previously investigated by Padhye et al. and Tunega et al. using density functional theory (DFT) are considered. This model assumes that the alumina shell of aluminum particles consists of several surface hydroxyl sites for both crystalline and amorphous surfaces. The interaction mechanism considers only the relatively elementary yet most energetically favorable exchange reaction, where a fluorine-bearing moiety mediates the replacement of terminal OH^- configurations by F^- in the formation of stronger Al−F bonds.[13,17,18] Based on past studies showing the presence of hydroxyl groups on metal oxides, it is further assumed, here, that the metal oxides in this study also consist of similar hydroxyl sites to that of alumina.[29−31] XRD analysis of MgO/PVDF in Figure 3d reinforces this point with an observation of crystalline $Mg(OH)_2$ on either its surface or interior.

One may surmise the exergonicity of the progression of metal oxide fluorination, or lack of fluorination, the behavior of HF fluorination of a general metal oxide based on simple Ellingham diagrams of standard Gibbs energies of formation for metal fluoride compounds relative to HF.[32,33] At room temperature, the Gibbs energies of formation of CuF_2, HF, BiF_3, MgF_2, AlF_3, TiF_4, and SiF_4 are ∼−480, −545, −565, −1045, −860, −730, and −755 kJ/mol of fluorine gas, respectively.[32,34] All values approach zero linearly as temper-

ature increases, except for HF whose Gibbs energy of formation decreases at a shallow rate to −565 kJ/mol at 1100 K (827 °C).[32,34] As temperature increases, the Gibbs energy of formation of CuF_2 increasingly deviates from that HF gas, indicating the low probability of stable CuF_2 ever forming relative to HF gas. In much of the same manner, MgF_2 and AlF_3 formation are extremely exergonic compared to HF at each respective temperature point of condensed phase analysis (Figure 3d,e) and are largely stable or likely to form after HF liberation from the polymer chain.

This same analysis approach is difficult to apply for the formation of BiF_3, TiF_4, and SiF_4 as their Gibbs energies are comparable to that of HF and their fluorination process appears slower and much more complex with the formation of metastable oxyfluorides in the cases for Bi_2O_3/PVDF and TiO_2/PVDF. A fraction of Bi_2O_3 fully reduces and produces CO_2 (Figure 3) much like CuO, albeit at a much slower rate, while TiO_2 has some of the earliest exotherms in DSC analysis but appears to be minimally affected in the condensed phase (no TiF_4 or TiF_3 observed) and eventually reverts to the more stable rutile structure after initially forming its oxyfluoride (Figure 3b,c). SiO_2 essentially has no change (Figure 3f). It should be noted that a major assumption of this analysis is that terminating hydroxyl sites are the primary mode of the fluorinating preignition reaction as exothermic reaction enthalpies are maximized at these locations.[18] Hydroxyl site considerations by Padhye et al. may add to this complexity as different types of hydroxyls sites require different energy amounts to break and depend heavily on crystal structure and oxygen vacancy.[17] Hydroxyl sites that form multiple bonds within vacated sites of TiO_2, Bi_2O_3, or any other similar metal oxide would make undergoing any substantial preignition fluorination process increasingly unlikely.

3.2. Rapid Heating Time-of-Flight Mass Spectrometry. Coupled T-jump/TOFMS of thinly coated metal oxide/PVDF sample on 76 μm Pt wire was used as a rapid heating and data acquisition tool to analyze, under combustion heating rates (10^5−10^6 K/s), pyrolysis products and intermediates. Both the intensity of HF and the potential effect that the inclusion of different metal oxides has on the overall profile of each mass spectrum are of primary focus where time resolution

of speciation is greatly enhanced over quadrupole mass spectrometer-based analysis.[28] The resulting full mass spectra averaged over a collection time of 10 ms from a 3 ms pulse heating at $\approx 3 \times 10^5$ K/s are displayed in Figure 4.

The PVDF control spectrum displays nearly identical mass spectrum patterns as observations conducted by previous PVDF pyrolysis experiments. As the main volatile, HF, appears in relatively large quantities, and main carbon chains are cleaved, several doubled-bonded fragmentations are formed at an accelerated rate.[14,27] More specifically, HF ($m/z = 20$), allylic ions ($m/z = 77, 95, 113$), alkyl ions ($m/z = 51, 65, 133$), the VDF monomer ($C_2F_2H_2$, $m/z = 64$), and their respective electron impaction fragmentations are observed in the measured mass spectrum.[27] Support for this pyrolysis mechanism initiated by HF release is demonstrated by time-dependent speciation of pyrolysis species in Figure S2, where HF gas is released ≈ 200 μs prior to the detection of higher mass species.

Most metal oxide/PVDF compositions in this study reflect the same general pyrolysis behavior as neat PVDF with the notable exception of Al_2O_3/PVDF whose unique mass spectrum does not contain any of the same higher mass species but instead releases species of $m/z = 132, 81, 49$, and 1. The degradation of PVDF generally separates itself from other hydrogenated fluoropolymers in theoretical models by the characteristic cyclization of depolymerized vinylidene fluoride to form trifluorobenzene ($C_6F_3H_3$; $m/z = 132$).[27] However, models of trifluorobenzene formation reflect a low probability of formation during pyrolysis given the assumptions of the degradation model and thus are not observed in corresponding experimental spectra.[27] The formation of trifluorobeneze in the case of Al_2O_3/PVDF suggests an alternative pyrolysis or interaction mechanism of PVDF with Al_2O_3, which may either be unique with respect to previously described degradation models or better fulfills the assumptions of such degradation models.[27] Given the lack of any other large mass species normally indicative of fluoropolymer degradation, the former appears more likely.

Prior studies have suggested that the availability and rate of HF release is likely a driving factor in the fluorination mechanism responsible for the reaction rate of propellant systems, where PVDF is the primary oxidizing agent.[2,17] Semiquantitative analysis of the release behavior of HF volatiles was conducted by measuring the maximum intensity of HF ($m/z = 20$) of each composition upon release relative to that of neat PVDF as a function of release temperature. These results are displayed in Figure 5.

A clear correlation is illuminated from this analysis where the relative intensity of released HF gas increases dramatically as the temperature of the release point decreases with Al_2O_3/PVDF separating itself above all others. The compositions that release HF in larger quantities than PVDF versus those that release less HF than PVDF reflect the same grouping of compositions via TGA-DSC analysis in Figure 2. This similarity seems to suggest the correlation between HF release and the progression of exothermic behavior. Despite this finding, a primary question now arises from this analysis: Does the larger HF intensity at lower temperature occur due to a more exothermic interaction that locally increases temperature for further HF release or does there exist some more fundamental surface interaction between the metal oxide surfaces and PVDF prior to HF release which allows HF gas to more easily be released?
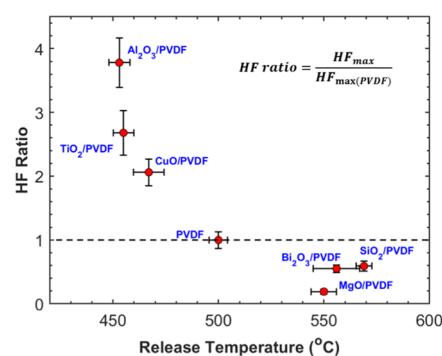

Figure 5. T-jump/TOFMS measured relative HF release maximum (HF ratio) of metal oxide/PVDF compositions as a function of release temperature.

The study conducted by Padhye et al. points out that a more crystalline shell of alumina acts as an upper limit in the reduction of the onset for the preignition reaction as crystalline shells have higher concentrations of hydroxyl termination and therefore a greater concentration of surface reactions with the highest potential exothermicity.[17,18] Since we cannot readily compare the degree of crystallinity between differing materials, this point maybe moot or incomplete. Our observations are more likely associated with surface interactions that both lower the onset temperature of HF release and its associated exothermicity offers feedback to promote further HF release, as illustrated in Figure 6. The distinction between the two is most evident in the behavior of MgO/PVDF and Al_2O_3/PVDF, as observed by Figures 2 and 5. MgO/PVDF releases very little HF following the onset temperature even though both materials react readily and exothermically with PVDF to form some of the most stable metal fluorides.

Further insight can be gained when T-jump/TOFMS results are analyzed in tandem with TGA and XRD findings. From TGA (Figure 2), the remaining mass fraction of a composite should theoretically be $\sim 60\%$ at 1000 °C if it is assumed that there is no interaction between metal oxide particles and PVDF. Bi_2O_3/PVDF has the largest mass loss (Figure 2), which is largely due to the O removal from Bi_2O_3 and evaporation of Bi as XRD shows a nearly full transformation from Bi_2O_3 to Bi (Figure 3b), and Bi^+ is observed in T-jump/TOFMS (Figure 5). The remaining mass of SiO_2/PVDF is about 10% lower than 60% (Figure 2); while XRD (Figure 3f) indicates that there is no change in composition, T-jump/TOFMS shows the presence of SiF_3^+ (fragment of SiF_4), which makes it likely that SiO_2 reacts with HF released from PVDF and results in the mass loss. The final mass fractions of TiO_2, Al_2O_3/PVDF, and MgO/PVDF are about 60%. While XRD shows a fraction of MgO and Al_2O_3 fully converts to MgF_2 and AlF_3, respectively, most of MgO and Al_2O_3 still remain (Figure 3d,e). As for TiO_2/PVDF, even though XRD shows a crystal structure change, the product is still TiO_2 (Figure 3c). Thus, there are no extra mass losses for these three composites.

Most interestingly, despite having shown no evidence for any form of fluorination at all, CuO/PVDF releases twice as much HF as neat PVDF at a lower temperature. CuO/PVDF has a remaining mass about 20% lower than 60% (Figure 2). The difference is attributed to the removal of O from CuO as well as the consumption of PVDF from the reaction with CuO/Cu_2O, with Cu as the only measured crystalline product. The primary exotherms in Figure 2a,b are attributed to the formation of CO_2 ($m/z = 44$), which is detected by mass
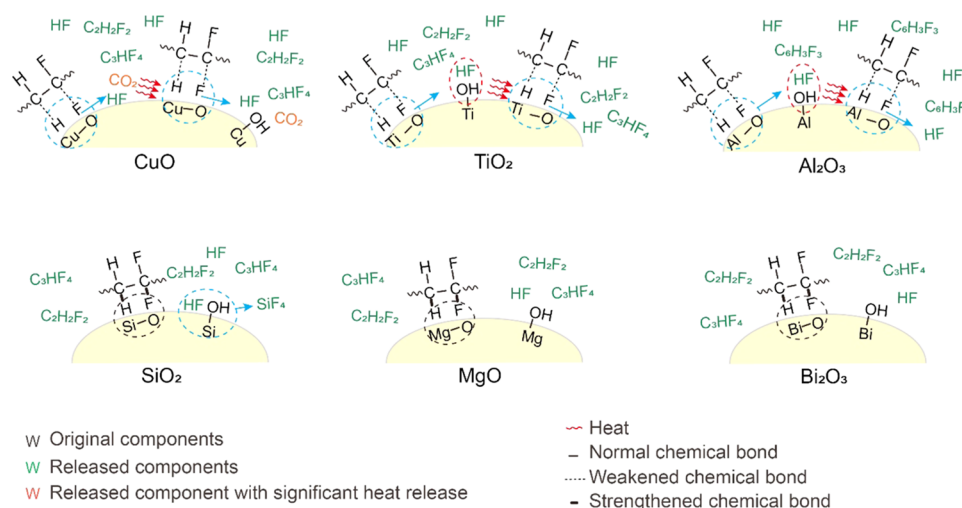
Figure 6. Initialization of the proposed interactions between the studied metal oxides and PVDF, where those on the top layer release far more HF gas and react with decomposing PVDF at early temperatures compared to neat PVDF decomposition.

spectrometry ≈200 μs prior to HF release (Figure S3).[28] Although T-jump/TOFMS of neat CuO nanoparticles, alone, releases CO_2 from the decomposition of naturally occurring copper carbonate (azurite or malachite),[21,35] the intensity of CO_2 detection by mass spectrometry in Figure 4 is far too strong to be explained by the decomposition of copper carbonate. The lack of oxygen intensity points to a reaction that directly takes place between oxygen originating in CuO/Cu_2O and PVDF prior to HF release. The exothermicity may then further drive HF release (Figure 6). The importance of this observation is not that HF was released in larger quantities than neat PVDF but that the exothermic event needed to drive that release need not be a fluorination event (Figure 6). CuO is driven to decompose to Cu_2O in a mass-independent manner nearly 500 °C earlier than what has been documented based on our TGA-DSC results in Figures 2 and S4.

A mutually beneficial degradation behavior is highlighted in the case of CuO/PVDF at slow heating rates (Figure S4) and may be generalized to other material compositions. Additionally, this behavior more broadly suggests a two-step process where surface proximity interactions for early-onset HF release and a relatively exothermic HF/metal oxide surface interaction are necessary to enhance fluorination progression.

4. CONCLUSIONS

This study investigates the role of nanoscale metal oxides (Al_2O_3, SiO_2, TiO_2, MgO, CuO, Bi_2O_3) in the pyrolysis of PVDF and subsequent interactions. The main volatile product from the pyrolysis of PVDF is HF gas that engages in previously proposed reactions with OH^- sites on metal oxide surfaces, replacing OH^- by F^- in the formation of stronger metal−fluorine bonds. However, corresponding stable metal fluoride may not be produced after the reaction. Analysis of the temperature-dependent condensed phase as well as volatile species progression shows that these compositions can mainly be divided into three groups: full transition to most stable fluorine compound (Al_2O_3/PVDF, MgO/PVDF, SiO_2/PVDF), metastable fluorination/oxyfluoride progression (TiO_2/PVDF, Bi_2O_3/PVDF), and no fluorination with enhanced reduction of metal oxide (CuO/PVDF). It is found that while Al_2O_3, TiO_2, and CuO enhance decomposition behavior and the HF release from PVDF, SiO_2, MgO,

and Bi_2O_3 suppress HF release and retard the onset of PVDF decomposition. The relative intensity of HF gas increases dramatically as the onset temperature of HF release decreases.

Compositions that release HF in larger quantities than PVDF demonstrate exothermic, multistep mass loss modes prior to neat PVDF mass loss, suggesting a correlation between HF release and the progression of exothermic behavior. We propose that interactions between HF promoting metal oxides both lower the activation energy of HF release and engage exothermically with HF gas to promote further local HF release. However, the release of HF gas may be facilitated by alternative exothermic behavior prior to PVDF decomposition, as shown by significant CO_2 formation preceding HF release in the case of CuO/PVDF.

Al_2O_3/PVDF separates itself from other compositions based on its unique T-jump mass spectrum, which produces the largest release of HF gas and generates trifluorobenzene instead of any of the other higher mass species observed in both neat PVDF and other compositions. Models of trifluorobenzene formation reflect a low probability of formation during pyrolysis, implying an alternative pyrolysis or interaction mechanism of PVDF with Al_2O_3. This suggests a potential difference in reaction mechanism, which requires more sophisticated models to illustrate the interaction of Al_2O_3 and PVDF and how this interaction fundamentally differs.

■ ASSOCIATED CONTENT

ⓢ Supporting Information

The Supporting Information is available free of charge at https://pubs.acs.org/doi/10.1021/acsami.1c20938.

> Figure S1: TEM of metal oxide nanoparticles; Figure S2: time-dependent full mass spectra of rapidly heated PVDF; Figure S3: time-dependent full mass spectra of rapidly heated CuO/PVDF; and Figure S4: CuO/PVDF TGA profile and the resulting rate of mass loss (PDF)

■ AUTHOR INFORMATION

Corresponding Author

Michael R. Zachariah − *Department of Chemical and Environmental Engineering, University of California, Riverside, Riverside, California 92521, United States;*

 orcid.org/0000-0002-4115-3324; Email: mrz@engr.ucr.edu

Authors

Miles C. Rehwoldt − *Department of Chemistry and Biochemistry, University of Maryland, College Park, Maryland 20742, United States; Department of Chemical and Environmental Engineering, University of California, Riverside, Riverside, California 92521, United States*

Yujie Wang − *Department of Chemical and Environmental Engineering, University of California, Riverside, Riverside, California 92521, United States*

Feiyu Xu − *Department of Chemistry and Biochemistry, University of Maryland, College Park, Maryland 20742, United States; Department of Chemical and Environmental Engineering, University of California, Riverside, Riverside, California 92521, United States*

Pankaj Ghildiyal − *Department of Chemistry and Biochemistry, University of Maryland, College Park, Maryland 20742, United States; Department of Chemical and Environmental Engineering, University of California, Riverside, Riverside, California 92521, United States;* orcid.org/0000-0002-4422-3068

Complete contact information is available at:
https://pubs.acs.org/10.1021/acsami.1c20938

Author Contributions

§M.C.R. and Y.W. are co-first authors.

Notes

The authors declare no competing financial interest.

■ REFERENCES

(1) Li, X.; Zachariah, M. R. Direct Deposit of Fiber Reinforced Energetic NanoComposites. *Propellants, Explos. Pyrotech.* **2017**, *42*, 1079−1084.

(2) Delisio, J. B.; Hu, X.; Wu, T.; Egan, G. C.; Young, G.; Zachariah, M. R. Probing the Reaction Mechanism of Aluminum/Poly-(Vinylidene Fluoride) Composites. *J. Phys. Chem. B* **2016**, *120*, 5534−5542.

(3) Song, J.; Guo, T.; Ding, W.; Yao, M.; Bei, F.; Zhang, X.; Huang, J.; Fang, X. Study on Thermal Behavior and Kinetics of Al/MnO2 Poly(Vinylidene Fluorine) Energetic Nanocomposite Assembled by Electrospray. *RSC Adv.* **2019**, *9*, 25266−25273.

(4) Lyu, J. Y.; Chen, S.; He, W.; Zhang, X. X.; Tang, D.; Liu, P. J.; Yan, Q. L. Fabrication of High-Performance Graphene Oxide Doped PVDF/CuO/Al Nanocomposites via Electrospinning. *Chem. Eng. J.* **2019**, *368*, 129−137.

(5) Sidebottom, M. A. Ultralow Wear Fluoropolymer Metal-Oxide Composites: Nanomechanics & Tribochemistry, 2018. *Theses and Dissertations*, 4251, https://preserve.lehigh.edu/etd/4251.

(6) Sengwa, R. J.; Dhatarwal, P.; Choudhary, S. A Comparative Study of Different Metal Oxide Nanoparticles Dispersed PVDF/PEO Blend Matrix-Based Advanced Multifunctional Nanodielectrics for Flexible Electronic Devices. *Mater. Today Commun.* **2020**, *25*, No. 101380.

(7) Dutta, B.; Kar, E.; Bose, N.; Mukherjee, S. Significant Enhancement of the Electroactive β-Phase of PVDF by Incorporating Hydrothermally Synthesized Copper Oxide Nanoparticles. *RSC Adv.* **2015**, *5*, 105422−405434.

(8) Martins, P.; Lopes, A. C.; Lanceros-Mendez, S. Electroactive Phases of Poly(Vinylidene Fluoride): Determination, Processing and Applications. *Prog. Polym. Sci.* **2014**, *39*, 683−706.

(9) Koch, E. C. Metal-Fluorocarbon-Pyrolants: III. Development and Application of Magnesium/Teflon/Viton (MTV). *Propellants, Explos. Pyrotech.* **2002**, *27*, 262−266.

(10) Crouse, C. A. Fluorinated Polymers as Oxidizers for Energetic Composites. *ACS Symp. Ser.* **2012**, *1106*, 127−140.

(11) Hendel, F. J. Review of Solid Prolleants for Space Exploration. *NASA Jet Propulsion Laboratory Technical Memorandum*, 1965.

(12) Wang, H.; Rehwoldt, M.; Kline, D. J.; Wu, T.; Wang, P.; Zachariah, M. R. Comparison Study of the Ignition and Combustion Characteristics of Directly-Written Al/PVDF, Al/Viton and Al/THV Composites. *Combust. Flame* **2019**, *201*, 181−186.

(13) Valluri, S. K.; Schoenitz, M.; Dreizin, E. Fluorine-Containing Oxidizers for Metal Fuels in Energetic Formulations. *Def. Technol.* **2019**, *15*, 1−22.

(14) Madorsky, S. I.; Hart, V. E.; Straus, S.; Sedlak, V. A. Thermal Degradation of Tetrafluoroethylene and Hydrofluoroethylene Polymers in a Vacuum. *J. Res. Natl. Bur. Stand.* **1953**, *51*, 327.

(15) Strutton, J. W.; Knott, M.; Bencomo, J. A.; Iacono, S. T.; Mates, J. E.; Alston, J. R.; McCollum, J. M. Manipulating Polymer Decomposition to Alter Burn Performance in Aluminium/Poly-(Vinylidene Fluoride) Filaments. *Polym. Int.* **2020**, *70*, 768−774.

(16) He, W.; Lyu, J. Y.; Tang, D. Y.; He, G. Q.; Liu, P. J.; Yan, Q. L. Control the Combustion Behavior of Solid Propellants by Using Core-Shell Al-Based Composites. *Combust. Flame* **2020**, *221*, 441−452.

(17) Padhye, R.; Aquino, A. J. A.; Tunega, D.; Pantoya, M. L. Fluorination of an Alumina Surface: Modeling Aluminum − Fluorine Reaction Mechanisms. *ACS Appl. Mater. Interfaces* **2017**, *9*, 24290−24297.

(18) Tunega, D.; Pantoya, M. L.; Nieman, R.; Lischka, H.; Aquino, A. J. A. Reaction Mechanism for Fluorination Reactions with Hydroxylated Alumina Sites: Pathways Promoting Aluminum Combustion Reaction Mechanism for Fluorination Reactions with Hydroxylated Alumina Sites: Pathways Promoting Aluminum Combustion. *J. Chem. Phys.* **2021**, *154*, No. 104308.

(19) Smith, D. W. J.; Iacono, S. T.; Iyer, S. S., Eds. *Handbook of Fluoropolymer Science and Technology*; John Wiley & Sons, Inc., 2014.

(20) Ma, X.; Li, Y.; Hussain, I.; Shen, R.; Yang, G.; Zhang, K. Core−Shell Structured Nanoenergetic Materials: Preparation and Fundamental Properties. *Adv. Mater.* **2020**, *32*, No. 2001291.

(21) Rehwoldt, M. C.; Wang, H.; Kline, D. J.; Wu, T.; Eckman, N.; Wang, P.; Agrawal, N. R.; Zachariah, M. R. Ignition and Combustion Analysis of Direct Write Fabricated Aluminum/Metal Oxide/PVDF Films. *Combust. Flame* **2020**, *211*, 260−269.

(22) Smith, D. K.; Unruh, D. K.; Wu, C. C.; Pantoya, M. L. Replacing the Al2O3 Shell on Al Particles with an Oxidizing Salt, Aluminum Iodate Hexahydrate. Part I: Reactivity. *J. Phys. Chem. C* **2017**, *121*, 23184−23191.

(23) Jian, G.; Zhou, L.; Piekiel, N. W.; Zachariah, M. R. Low Effective Activation Energies for Oxygen Release from Metal Oxides: Evidence for Mass-Transfer Limits at High Heating Rates. *ChemPhysChem* **2014**, *15*, 1666−1672.

(24) Zarko, V. E.; Knyazeva, A. G. Determination of Kinetic Parameters of Exothermic Condensed Phase Reaction Using the

Energetic Material Ignition Delay Data. *Combust. Flame* **2020**, *221*, 453−461.

(25) Rehwoldt, M. C.; Yang, Y.; Wang, H.; Holdren, S.; Zachariah, M. R. Ignition of Nanoscale Titanium/Potassium Perchlorate Pyrotechnic Powder: Reaction Mechanism Study. *J. Phys. Chem. C* **2018**, *122*, 10792−10800.

(26) Juibari, N. M.; Eslami, A. Investigation of Catalytic Activity of ZnAl2O4 and ZnMn2O4 Nanoparticles in the Thermal Decomposition of Ammonium Perchlorate: Structural and Kinetic Studies. *J. Therm. Anal. Calorim.* **2017**, *128*, 115−124.

(27) Lonfei, J.; Jingling, W.; Shuman, X. Mechanisms of Pyrolysis of Fluoropolymers. *J. Anal. Appl. Pyrolysis* **1986**, *10*, 99−106.

(28) Li, X.; Huang, C.; Yang, H.; Li, Y.; Cheng, Y. Thermal Reaction Properties of Aluminum/Copper (II) Oxide/Poly(Vinylidene Fluoride) Nanocomposite. *J. Therm. Anal. Calorim.* **2016**, *124*, 899−907.

(29) Zaki, M. I.; Knozinger, H. Carbon Monoxide - A Low Temperature Infrared Probe for Charcterization of Hydroxyl Group Properties on Metal Oxide Surfaces. *Mater. Chem. Phys.* **1987**, *17*, 201−215.

(30) McCafferty, E.; Wightman, J. P. Determination of the Concentration of Surface Hydroxyl Groups on Metal Oxide Films by a Quantitative XPS Method. *Surf. Interface Anal.* **1998**, *26*, 549−564.

(31) Tamura, H.; Tanaka, A.; Mita, K.; Furuichi, R. Surface Hydroxyl Site Densities on Metal Oxides as a Measure for the Ion-Exchange Capacity. *J. Colloid Interface Sci.* **1999**, *209*, 225−231.

(32) Howard, S. M. *Ellingham Diagrams*; SD School of Mines and Technology, 2006.

(33) *CRC Handbook of Chemistry and Physics*; In Lide, D. R., Ed.; CRC Press: Boca Raton, FL, 2005.

(34) Yoo, J.-H.; Lee, B.-G.; Kang, Y.-H.; Kim, E.-H.; Kwon, S.-W.; Shim, J.-B.; Ahn, B.-G.; Woo, M.-S.; Hwang, S.-C.; Park, J.-H., et al. Thermodynamic Data-Base for Metal Fluorides. *Korea Atomic Energy Research Institute Report*, 2001.

(35) Mansour, S. A. A. Thermoanalytical Investigations of Decomposition Course of Copper Oxysalts - I. Basic Copper Carbonate. *J. Therm. Anal.* **1994**, *42*, 1251−1263.